Final Technical Report: Award Number G19AP00020 Investigation the Seismic Signature of Earthquake Nucleation with Dynamic Simulations of Microearthquakes

Camilla Cattania, Paul Segall
Stanford University

May 2020

Abstract

Since first proposed by Aki (1967), the concept of earthquake self-similarity has been the subject of intense debate. While observations suggesting a break in self-similarity have been reported (Harrington and Brodsky, 2009; Bouchon et al., 2011; Lin et al., 2016; Imanishi and Uchide, 2017), it is well known that artifacts can arise due to attenuation of high-frequencies (Abercrombie, 1995; Ide et al., 2003). The constant improvement of seismic catalogs will offer the chance to observe microseismicity, possibly down to the nucleation dimension, and an improved theoretical understanding of the source characteristics near nucleation is required to interpret these datasets.

To this end, we use dynamic simulations and ideas from fracture mechanics to derive a source model for earthquakes with sizes near the nucleation dimension. Self-similar models, such as those proposed by Madariaga (1976) and Sato and Hirasawa (1973), assume that ruptures start as a point and propagate at constant velocity. In contrast, frictional theory predicts the existence of a *finite* nucleation length (Ruina, 1983; Rubin and Ampuero, 2005): slip velocities increase over the nucleation area, and rupture velocity increases from zero to its limiting value. We run dynamic simulations of earthquake cycles on circular asperities loaded by creep, with dimensions between 1 and 2 critical nucleation lengths. In this size range, creep penetrates inwards and reaches the center of the asperity, where ruptures begin. We identify two types of ruptures: first a brief acceleration, barely seismic, with slip velocities decaying as it expands; then a larger rupture, releasing most of the seismic moment and expanding as a constant stress drop crack. Surprisingly, we find that far-field ground motion pulses show nearly constant duration, independent of the asperity radius; this is confirmed by constant corner frequencies derived from synthesized source spectra.

To explain this behavior, we derive an equation of motion for accelerating circular ruptures based on an energy balance: the *dynamic* energy release rate, which is a function of crack size and rupture velocity, must equal the fracture energy (in our case, a constant). In the early phases of nucleation, we find that rupture velocity increases exponentially with time, and since the crack area grows slowly, the same time dependence is reflected in synthetic far-field ground motion. Due to the exponential growth, theoretical far-field pulses for events of different size collapse on the same curve once normalized, giving rise to the apparent constant duration found in the numerical simulations. These results imply: 1) that source duration is not a reliable proxy for rupture dimension near the nucleation length, and 2) that the break in self-similarity would

manifest as an apparent decrease in stress drop for smaller earthquakes since their relative size is overestimated.

1 Methods

We run fully dynamic simulations using the boundary integral code *BICyclE* (Lapusta et al., 2000; Lapusta and Liu, 2009). The following equation of motion governs fault slip:

$$\tau_{el}(\mathbf{x}) - \tau_f(\mathbf{x}) = \frac{\mu}{2c_s} v(\mathbf{x}), \tag{1}$$

where μ is the shear modulus, τ_f the frictional resistance, τ_{el} the shear stress due to remote loading and elastodynamic stress interactions between elements, and the term on the right hand side represents radiation damping (Rice, 1993). Frictional resistance evolves according to rate-state friction (Marone, 1998):

$$\tau_f(v, \theta) = \sigma \left[f_0 + a \log \frac{v}{v^*} + b \log \frac{\theta v^*}{d_c} \right], \tag{2}$$

where, a, b and are constitutive parameters; d_c is the state evolution distance; σ is effective the normal stress; v_0 is a reference slip velocity; f_0 is the steady-state friction coefficient at $v = v^*$, and θ is a state-variable. We employ the ageing law (Ruina, 1983) for state evolution:

$$\frac{d\theta}{dt} = 1 - \frac{\theta v}{d_c}. \tag{3}$$

We impose velocity weakening frictional parameters ($a - b = -0.05$, $b = 0.02$) within a circular asperity, and velocity strengthening parameters ($a - b = 0.05$) outside of it. The fault is loaded by a velocity boundary condition. Nucleation under ageing law with the parameters employed here is expected to take the form of an expanding crack with the nucleation dimension given by:

$$R_\infty = \frac{\pi}{4} \frac{b}{(b-a)^2} \frac{\mu' d_c}{\sigma} \tag{4}$$

where μ' is the shear modulus for antiplane shear and the shear modulus divided by $1 - \nu$ (ν = Poisson's ratio) for plane strain deformation. This is analogous to the nucleation dimension obtained by (Rubin and Ampuero, 2005) for 2D cracks.

To derive far-field pulses and spectra from fault slip we use the following results (Aki and Richards, 1980):

$$u(\mathbf{x}, t) = \alpha \int_{source} v(t - d(r, \varphi)/c)\ r\ d\varphi\ dr \tag{5}$$

where v is the slip velocity, c the wave velocity, $d(r, \varphi)$ the distance between the receiver and a point on the source, and A a constant including the radiation pattern for P- and S-waves, and geometrical spreading. In what follows, we restrict our attention to an observer at $\theta = 0$, where θ is the angle from the axis of the asperity; other orientations will be the considered in future work.

2 Results

Two types of seismic ruptures

Fig. 1 shows an example of a cycle for $R = 1.2R_\infty$. As previously noted by Chen and Lapusta (2009), as the creep front coalesces towards the center of the asperity it accelerates, reaching

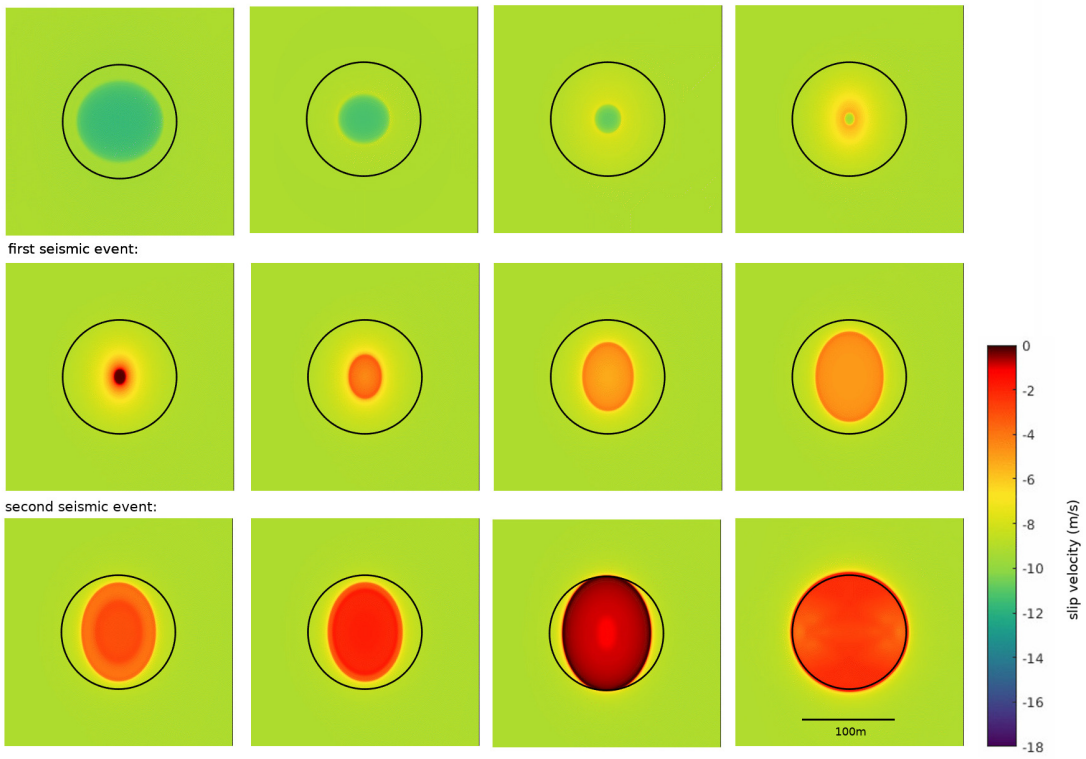

Figure 1: Example of simulations showing an earlier rupture with slip velocities decaying as it expands (middle row) followed by a larger crack-like rupture.

seismic slip velocities over a small area (several times smaller than R_∞). This rupture dies out as it expands. The two smallest asperities ($R \leq 1.05R_\infty$) only produce this type of rupture; in contrast, larger asperities produce a second rupture style with the characteristics of the expanding crack identified by Rubin and Ampuero (2005). The time between the two ruptures is of the order of minutes: much smaller than the cycle duration but much greater than each individual rupture (Fig. 3). The second rupture has a longer duration and it releases about 100 times more seismic moment than the first one (Fig. 2). Its spectrum appears similar to a Brune spectrum (although some small deviations exist, as discussed in the following section): flat at low frequency and decaying as $1/f^2$ at high frequencies. In contrast, we find that smaller events have a decaying power spectrum even at low frequencies (Fig. 2).

In the remaining part of the report we focus on the second rupture, since it releases most of the moment and is more likely to be observed in nature.

Source spectra

We calculated far-field ground motion and source spectra as describe in section 1. First, we fit a Brune model to the spectrum, estimating both n and f_c; however, we note that the spectrum presents a slight decay at low frequencies, and the corner frequency tends to be underestimated by assuming a Brune spectrum. Therefore we assume a spectrum of the form:

$$A(f) = \frac{f^m}{1 + (f/f_c)^n}, \tag{6}$$

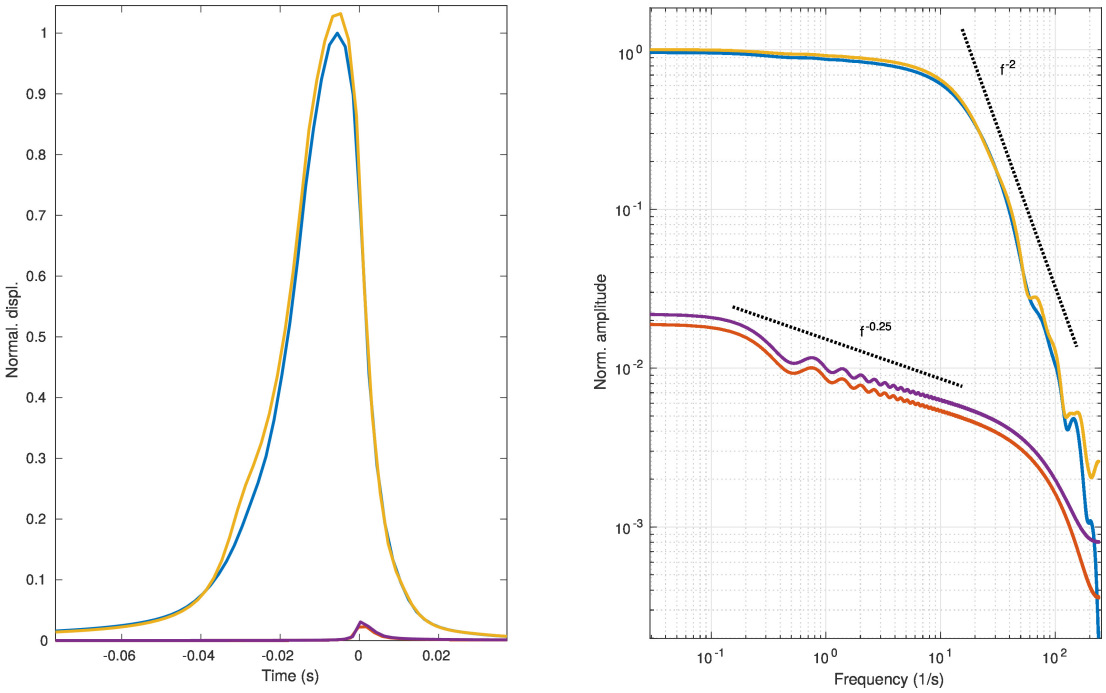

Figure 2: Far field ground motion (left) and source spectra (right) for 4 consecutive ruptures, normalized by the amplitude of the last rupture.

and fit n, m and f_c.

Fig. 4 shows normalized far-field ground motion and source spectra for sources with a radius between $R = 1.1R_\infty$ and $R = 2R_\infty$. As expected, the rupture on the largest asperity ($R = 2R_\infty$) has a longer duration than the others; surprisingly, all other events appear to have approximately the same duration. The constant duration can also be seen in the spectra and estimated corner frequencies, which do not scale with moment as expected from a self-similar model ($f_c \sim M_0^{-1/3}$) but are instead nearly constant, except for the largest asperity. The increase in rupture duration and decrease in corner frequency for the largest asperity is due to the transition between central ruptures and lateral ruptures, expected to occur at $R \sim 2R_\infty$ (Cattania and Segall, 2019). As expected, the corner frequency decreases by about a factor of two, since the rupture has to propagate a distance $2R$ for ruptures nucleating at the edge compared to those that start at the asperity center.

A source model for accelerating ruptures

The classical scaling between rupture dimension and duration follows from the assumption of constant rupture velocity; this assumption breaks down during nucleation, as the rupture front accelerates. To understand earthquake duration vs. source dimension in this regime we need an equation of motion for the rupture front, which we derive from fracture mechanics. Following Freund (1990), we treat the rupture as a crack, where the motion of the crack tip is controlled by balance between the mechanical energy provided by slip behind the crack tip, and the fracture energy:

$$G(r, \dot{r}) = \Gamma, \tag{7}$$

where Γ is the fracture energy and G the dynamic energy release rate, which is a function of the rupture dimension and rupture velocity. The latter is related to the stress intensity factor

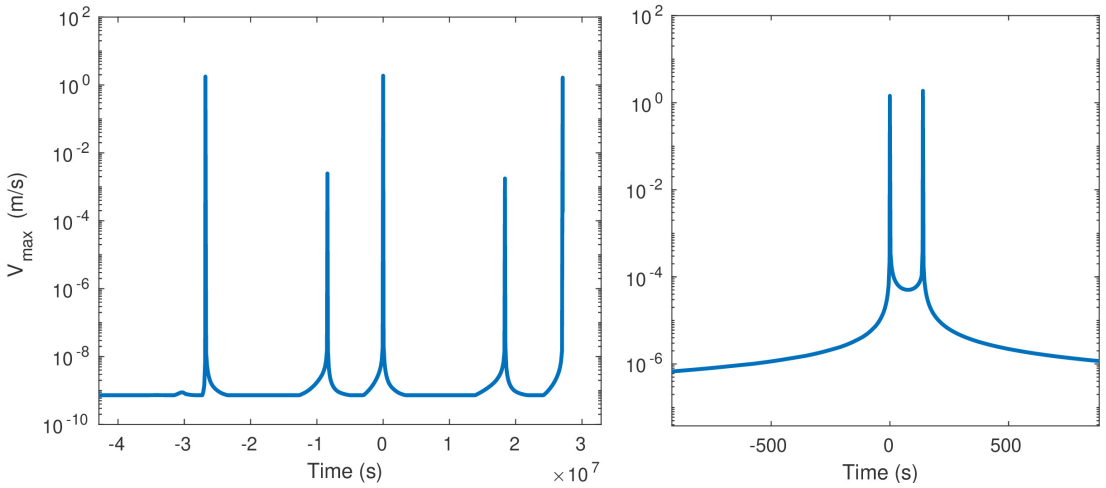

Figure 3: Maximum slip speed vs. time on the asperity with $R = 1.2R_\infty$, showing aseismic ruptures (e.g. at time $t \sim -10^7$s) followed by two ruptures within a short time ($t \sim 0$).

by

$$G = A(\dot{r})\frac{K(r,\dot{r})^2}{2\mu'}, \tag{8}$$

where A, is a universal function of crack speed (different for each mode of deformation); $K(r,\dot{r})$ is the dynamic stress intensity factor, which can be written as

$$K(r,\dot{r}) = k(\dot{r})K(r,0), \tag{9}$$

where $K(r,0)$ is the static stress intensity factor and $k(\dot{r})$ a universal function of rupture velocity. For simplicity of notation, we write the static stress intensity factor as $K(r)$. The equation of motion of the crack tip is then given by

$$K(r) = \left(\frac{2\mu\Gamma}{A(\dot{r})k(\dot{r})^2}\right)^{1/2}. \tag{10}$$

The product $A(\dot{r})k^2(\dot{r})$ can be approximated as $1 - \dot{r}/v$, where c is the shear wave velocity for mode III cracks and the Rayleigh wave velocity for mode II cracks. For simplicity, in what follows we neglect the difference between mode II and mode III, and assume that the crack is circular; the same results, within a factor of order one, are expected to apply for the elliptical crack in the case of mixed-mode propagation.

We assume the initial crack radius satisfies eq. 10 for $\dot{r} = 0$ (this is analogous to how Rubin and Ampuero (2005) derived R_∞). Eq. 10 can then be written as

$$K(r) = \frac{K(r_0)}{\sqrt{1 - \dot{r}/c}}. \tag{11}$$

The stress intensity factor for a circular crack of radius r is $K(r) \propto \Delta\tau\sqrt{r}$; assuming a constant stress drop and plugging this into eq. (11) yields the following expression for crack tip velocity as a function of radius:

$$V_r(r) = \dot{r} = c\left(1 - \frac{r_0}{r}\right). \tag{12}$$

Note that since $V_r(r_0) = 0$, solving for crack position as a function of time with initial condition $r(0) = r_0$ gives $r(t) = r_0$ at all times. Instead, we assume that the crack exceeds the nucleation

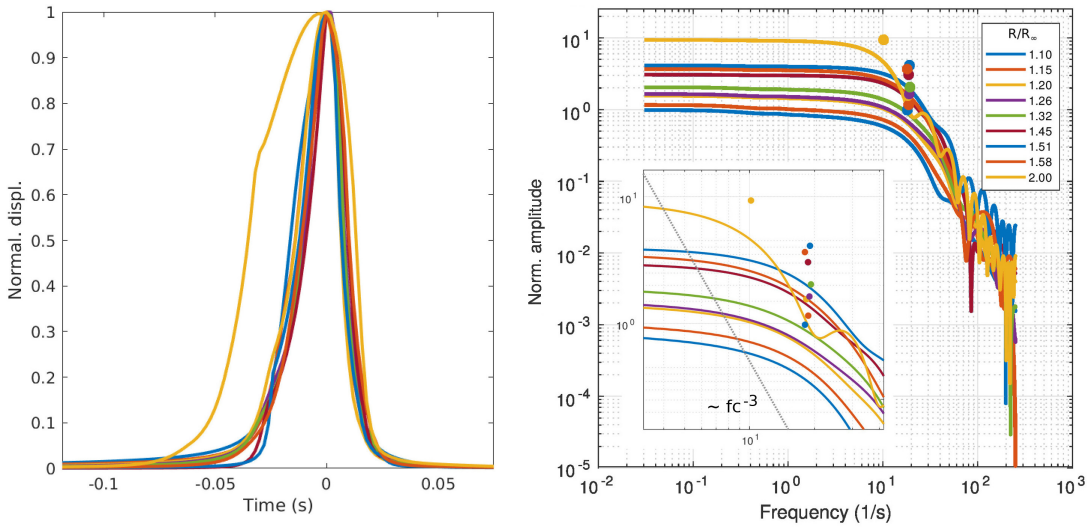

Figure 4: Normalized far-field displacements (left) and spectra (right) for events on ruptures with asperities between $1.1 - 2R_\infty$. All asperities except the largest one (in yellow) experience central ruptures, with constant duration and corner frequency.

dimension by a small amount: $r/r_0 = 1 + \epsilon$, with $\epsilon \ll 1$. The crack radius then grows as

$$r/r_0 = 1 + W\left(g \exp\left(t/t_0\right)\right) \quad (13)$$

$$\dot{r}/c = 1 - \left[1 + W\left(g \exp\left(t/t_0\right)\right)\right]^{-1} \quad (14)$$

where $W(\cdot)$ is the Lambert omega function, $t_0 = r_0/c$ is a characteristic timescale, and $g = W^{-1}(\epsilon) \approx \epsilon$. Fig. 5 shows that this expression is a reasonably good fit to the crack growth in the simulations for the mode III direction; the mode II direction is less well explained, since the initial radius in the simulations in smaller than the value predicted by eq. (4) and rupture velocities for a given radius are therefore underestimated.

Far-field pulses and source spectra for accelerating cracks

We are now in a position to model the far-field ground motion and source spectra for an accelerating crack. We start from the model proposed by Sato and Hirasawa (1973), which consists of a constant stress drop circular crack propagating with rupture velocity v_{rup}; however, here we relax the assumption of constant rupture velocity, and instead use the equation of motion derived in the previous section. Note that both the original and our modified version of the Sato and Hirasawa (1973) model do not include rupture arrest, and hence produce abrupt termination in far-field pulses. To address this limitation, in the future we will use the energy arguments in the previous section to derive an equation of motion for the rupture front as it enters a velocity strengthening region and eventually arrests.

A constant stress drop crack propagating at speed $V_r = \dot{r}$ has the following velocity profile:

$$V(\rho) = \frac{24\Delta\tau}{7\pi\mu'} \frac{r(t)}{\sqrt{r(t)^2 - \rho^2}} V_r(t), \quad (15)$$

where $\Delta\tau$ is the stress drop and $r(t)$ the crack radius, and ρ radial distance within the crack(Sato and Hirasawa, 1973). We use the expressions derived above for $r(t)$, $V_r(r)$ and calculate the

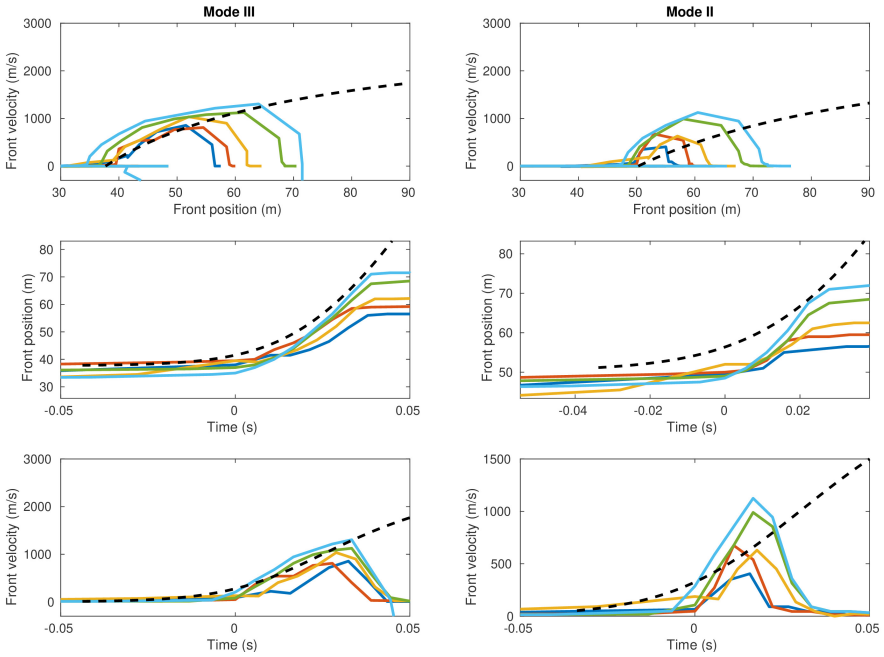

Figure 5: Top: rupture front velocity as function of crack radius: simulated events (colored lines) and theoretical expression (black). Middle, Bottom: Front position and velocity vs. time. Front position is identified by the peak in shear stress.

far-field motion from eq. 5. Fig. 7 shows the resulting normalized far-field spectra for the Sato and Hirasawa model with constant rupture velocity and our accelerating rupture model. As expected, the classic model assuming constant rupture velocity produces pulses of increasing duration, and thus decreasing corner frequency, with increasing R. In contrast, the accelerating model produces longer pulses due to the slower average rupture velocity. We also see that the duration of normalized pulses increases very slowly with radius.

Far-field spectra are proportional to the integrated slip speed (eq. 5), given by (15). For the observation angle $\theta = 0$ and in the far field, the time delay in eq. (5) is a constant, and the observed displacement is simply proportional to the integrated slip velocity. It can easily be shown that the integral is proportional to the product of crack area and rupture velocity:

$$u \sim \alpha r(t)^2 V_r(t). \tag{16}$$

where we omitted the time delay d/c in eq. (5) for notational convenience. For constant rupture velocity, far field displacements simply grow as rupture area or t^2. Once far-field motion is normalized by the final (maximum) displacement u_f and aligned at the end time of the rupture (as in Fig. 6) we get

$$\frac{u}{u_f} = \left(\frac{R/V_r - \Delta t}{R/V_r} \right)^2, \tag{17}$$

shown by the dotted lines in Fig. 6. If we define rupture duration as the time during which the normalized slip speed exceeds a certain value, it follows that $\Delta t \sim R/V_r$, as expected.

For the accelerating crack, both r and V_r are time-dependent; early on, $V_r \approx 0$ and we can assume that the radius is approximately constant, so that the duration of far-field displacement

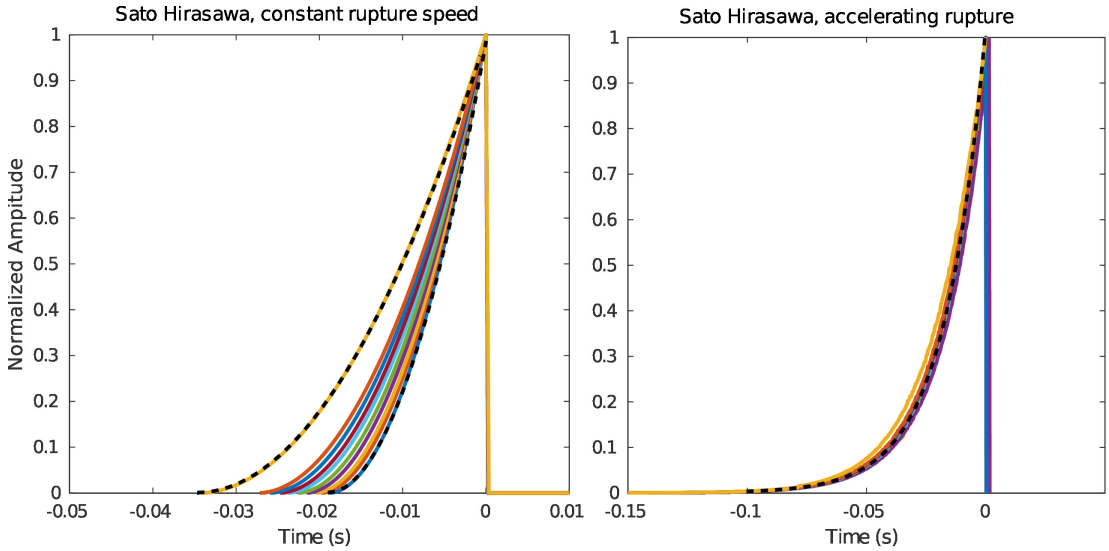

Figure 6: Semi-analytical far-field displacements, observed at $\theta = 0$ (e.g. along the asperity axis). Left: original Sato and Hirasawa (1973) model with constant rupture velocity. Right: modified model accounting for accelerating rupture. Colors correspond to the same R/R_∞ as Fig. 4. Black dotted lines are theoretical expressions derived assuming constant rupture velocity and $\approx$ constant radius respectively. Note the different scales on the x-axis.

is proportional to the rupture velocity, given by eq. 14. In the early stages of nucleation, when $g\exp(t/t_0) \ll 1$, the Lambert W-function can be approximated as $W(x) \approx x$ for $x \ll 1$ and we get

$$\dot{r}/c \approx g\exp\left(t/t_0\right). \tag{18}$$

The ratio between far-field displacements observed at a time Δt before the end of the rupture is then simply

$$\frac{u}{u_f} = \frac{V_r}{V_{r,f}} = \exp(-\Delta t/t_0), \tag{19}$$

and it does *not* depend on the final radius but only on the time interval, so that all normalized curves collapse on the same line. This expression, shown by the dotted lines in Fig. 6, is in excellent agreement with the model and it explains the constant rupture duration observed for events near the nucleation dimension.

Finally, we compare the corner frequencies from the original and modified Sato and Hirasawa (1973) model to the simulations (Fig. 7). While the original model predicts $f_c \sim 1/R$, our modified model reproduces the nearly constant corner frequency in the simulations.

3 Conclusion

We used fully dynamic rupture simulations and analytical results from fracture mechanics to derive a source model for small earthquakes, which accounts for acceleration in slip and rupture velocity as well as the finite size of the nucleation region. In the early phases of nucleation, analytical model predicts that far field displacements grows exponentially with time, producing a constant source duration and corner frequency.

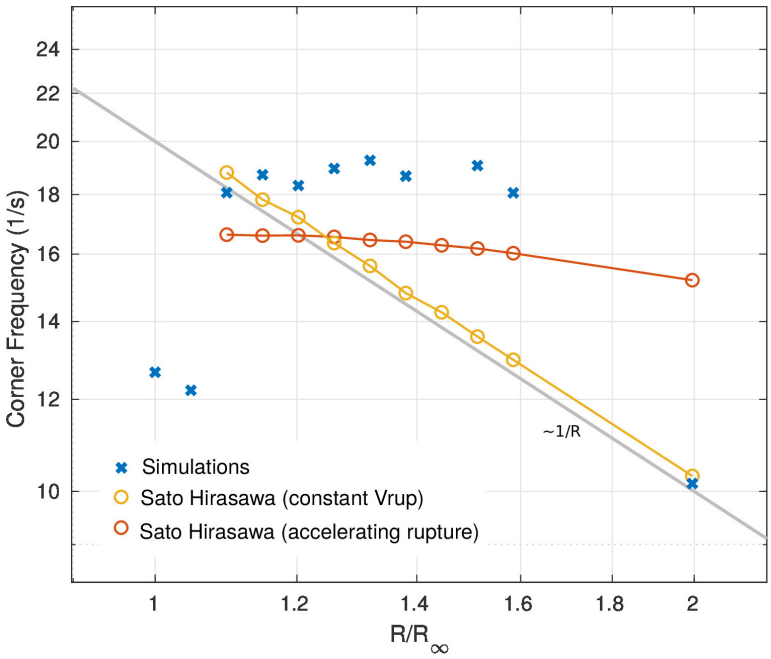

Figure 7: Corner frequencies vs. source dimension for simulated events (note that the two smallest asperities only experience small decaying ruptures, and not the crack-like ruptures we discuss here; and the largest asperity ruptures laterally). The classic Sato and Hirasawa (1973) model predicts $f_c \sim 1/R$, while the modified model accounting for acceleration produces constant f_c as observed in the simulations.

In terms of seismological observations, we therefore expect that the break in self-similarity would result in constant source duration for events approaching the nucleation dimension. The source radius estimated from classical methods would be overestimated, leading to an apparent low stress drops for small magnitude events.

Acknowledgements

We would like to thank Nadia Lapusta for sharing her *BICyclE* code and Valère Lambert for helping set up the simulations.

References

Abercrombie, R. E. (1995). Earthquake source scaling relationships from -1 to 5 M_l using seismograms recorded at 2.5-km depth. *Journal of Geophysical Research*, 100(B12):24015–24036.

Aki, K. (1967). Scaling law of seismic spectrum. *Journal of Geophysical Research*, 72(4):1217–1231. ISBN: 0148-0227.

Aki, K. and Richards, P. (1980). *Quantitative Seismology: Theory and Methods*. New York.

Bouchon, M., Karabulut, H., Aktar, M., Özalaybey, S., Schmittbuhl, J., and Bouin, M. P. (2011). Extended nucleation of the 1999 Mw 7.6 Izmit earthquake. *Science*, 331(6019):877–880. ISBN: 1095-9203 (Electronic)\r0036-8075 (Linking).

Cattania, C. and Segall, P. (2019). Crack models of repeating earthquakes predict observed moment-recurrence scaling. *Journal of Geophysical Research: Solid Earth*, 124(1):476–503.

Chen, T. and Lapusta, N. (2009). Scaling of small repeating earthquakes explained by interaction of seismic and aseismic slip in a rate and state fault model. *Journal Geophys. Res.*, 114:1–12.

Freund, L. B. (1990). *Dynamic Fracture Mechanics*. Cambridge Monographs on Mechanics.

Harrington, R. M. and Brodsky, E. E. (2009). Source duration scales with magnitude differently for earthquakes on the San Andreas fault and on secondary faults in Parkfield, California. *Bulletin of the Seismological Society of America*, 99(4):2323–2334. ISBN: 0037-1106.

Ide, S., Beroza, G. C., Prejean, S. G., and Ellsworth, W. L. (2003). Apparent break in earthquake scaling due to path and site effects on deep borehole recordings. *Journal of Geophysical Research: Solid Earth*, 108(B5). ISBN: 0148-0227.

Imanishi, K. and Uchide, T. (2017). Non-self-similar source property for microforeshocks of the 2014 Mw 6.2 Northern Nagano, central Japan, earthquake. *Geophysical Research Letters*, 44(11):5401–5410.

Lapusta, N. and Liu, Y. (2009). Three-dimensional boundary integral modeling of spontaneous earthquake sequences and aseismic slip. *Journal of Geophysical Research: Solid Earth*, 114(B9). _eprint: https://onlinelibrary.wiley.com/doi/pdf/10.1029/2008JB005934.

Lapusta, N., Rice, J. R., Ben-Zion, Y., and Zheng, G. (2000). Elastodynamic analysis for slow tectonic loading with spontaneous rupture episodes on faults with rate- and state-dependent friction. *Journal of Geophysical Research: Solid Earth*, 105(B10). Publisher: John Wiley & Sons, Ltd.

Lin, Y. Y., Ma, K. F., Kanamori, H., Alex Song, T. R., Lapusta, N., and Tsai, V. C. (2016). Evidence for non-self-similarity of microearthquakes recorded at a Taiwan borehole seismometer array. *Geophysical Journal International*, 206(2):757–773.

Madariaga, R. (1976). Dynamics of an expanding circular fault. *Bulletin of the Seismological Society of America*, 66(3):639–666. ISBN: 0037-1106.

Marone, C. (1998). Laboratory-derived friction laws and their application to seismic faulting. *Annual Review of Earth and Planetary Sciences*, 26(1):643–696.

Rice, J. R. (1993). Spatio-temporal complexity of slip on a fault. *Journal of Geophysical Research*, 98(B6):9885. ISBN: 2156-2202.

Rubin, A. M. and Ampuero, J. (2005). Earthquake nucleation on (aging) rate and state faults. *Journal of Geophysical Research*, 110(2):1–24.

Ruina, A. (1983). Slip instability and state variable friction law. *J. Geophys. Res.*, 88:10359–10370. ISBN: 0148-0227.

Sato, T. and Hirasawa, T. (1973). Body wave spectra from propagating shear cracks. *Journal of Physics of the Earth*, 21:415–431. ISBN: 0022-3743.